CHAPTER W15

Dielectric and Ferroelectric Materials

W15.1 Capacitors

Improvement in the design of capacitors has progressed steadily since the introduction of the Leyden jar in the nineteenth century. The basic formula for the capacitance of a parallel-plate capacitor is $C = \epsilon_r \epsilon_0 A/d$, where ϵ_r is the dielectric constant, A the surface area of a plate, and d the gap distance between plates. To increase C one either increases ϵ_r, increases A, or decreases d. Early capacitors consisted of metal foils separated by wax ($\epsilon_r \approx 2.5$), mica ($\epsilon_r \approx 3$ to 6), steatite ($\epsilon_r \approx 5.5$ to 7.5), or glass ($\epsilon_r \approx 5$ to 10). The use of titania (rutile) provided a significant increase ($\epsilon_{r_\parallel} = 170$, $\epsilon_{r_\perp} = 86$). This was followed by technology based on the perovskites, such as barium titanate ($\epsilon_r \approx 1000$), whose dielectric constant varies rapidly with temperature, undergoing a near divergence at a phase transition temperature. By going to smaller grain sizes (≈ 1 μm) the divergence was spread out over a larger temperature range, making the $\epsilon_r(T)$ curve flatter. Such perovskites are called *relaxors*. DRAM chips currently utilize capacitors with Si_3N_4 or SiO_2 as the dielectric material. The electrodes are made of doped Si or poly-Si.

The demands for miniaturization largely preclude an increase in the face area A. One exception is the multilayer ceramic capacitor (MLCC), in which case $C = \epsilon_r \epsilon_0 A(N-1)/d$, where N is the number of stacked plates. Electrolytic capacitors are successful in increasing C by reducing the gap distance d to atomic dimensions. In this case the dielectric consists of a monolayer of alumina ($\epsilon_r \approx 4.5$ to 8.4) or tantalum oxide (Ta_2O_5) ($\epsilon_r \approx 21$) sandwiched between a metal and an ionic solution. The inherent difficulty, however, is that electrolytic capacitors work only when polarized in one direction. The oxide layer disappears when the polarity is reversed. This makes them suitable for dc power supplies but not for ac applications. The development of thin-film technology provides another avenue of approach for reducing d. The material SiO ($\epsilon_r \approx 6$) provides a convenient dielectric. SiO is a "mixture" or alloy of Si and SiO_2 (e.g., oxygen-deficient SiO_{2-x}, with $x \approx 1$).

The MLCC typically uses $BaTiO_3$ as the dielectric, although it has some shortcomings. Ideally, the dielectric should have a low electrical conductivity so that the leakage current is not too large. The time constant for decay of charge in a dielectric is given by $\tau = \epsilon/\sigma$. (This formula may be deduced from Gauss's law, $\nabla \cdot \mathbf{D} = \rho$, the constitutive equations $\mathbf{D} = \epsilon\mathbf{E}$ and $\mathbf{J} = \sigma\mathbf{E}$, and the continuity equation $\partial\rho/\partial t + \nabla \cdot \mathbf{J} = 0$.) For high-speed switching applications it is desirable to have $\tau < 1$ μs. For $\sigma = 1\ (\Omega \cdot \text{m})^{-1}$ and $\epsilon = \epsilon_0$, the time constant is only 8.85×10^{-12} s. To obtain a 1-μs storage time requires ϵ/σ to be increased by over five orders of magnitude. It is also desirable to have a high thermal conductivity to avoid the buildup of thermal stresses, a high breakdown strength ($> 4 \times 10^7$ V/m) so that moderate voltages (≈ 200 V) can be imposed across

a small thickness (≈ 5 μm), as well as a capacitance that will not vary appreciably with electric field. One would like to have $d \approx 0.5$ μm, or less, if possible. Current research indicates that $d \approx 10$ μm may soon be feasible. A low dissipation factor is generally sought. The dissipation factor is defined as the ratio of the imaginary part of the dielectric constant to the real part, and is also referred to as the *loss tangent*, $\tan\delta \equiv \epsilon_2/\epsilon_1$. A low firing temperature and a small grain size for the ceramic are assets. A list of typical dielectrics (relaxors) is presented in Table W15.1. The value of the structural phase transition temperature T_c is presented, along with the value of the relative dielectric constant at that temperature. The closer the value of T_c is to room temperature, the higher the value of the dielectric constant will be under normal operating conditions. Much of the research in developing relaxor dielectrics has been aimed at tuning the stoichiometric coefficients to bring T_c close to room temperature. This is illustrated by the perovskite $Pb_{1-x}La_x(Zr_yTi_{1-y})_{1-x/4}O_3$ (PLZT) in Table W15.1. Changing the composition (x, y) from (0.02,0.65) to (0.08,0.7) lowers T_c from 320°C to 20°C and changes ϵ_r at T_c from 4050 to 650. Typical room temperature values of ϵ_r for ($SrTiO_3$, (Ba,Sr)TiO_3, PLZT) are (90–240,160–600, $>$ 1000), respectively.

Electrode materials for use with the perovskites include the metals Ir, Pt, Ru and the conducting oxides RuO_2 and IrO_2.

Grain-boundary barrier layer (GBBL) capacitors achieve a high capacitance essentially by decreasing d. The dielectric consists of a set of microscopic conducting granules, of typical size a, separated from each other by thin insulating surface layers, of dimension d_g. The average number of grains spanning the gap is N. Using $Na + (N+1)d_g = d$, one finds that $N = (d - d_g)/(a + d_g) \approx d/a$. The net capacitance is obtained by regarding the $N + 1$ capacitors as being in series, resulting in

$$C = \epsilon_r\epsilon_0 \frac{A}{Nd_g} = \epsilon_r\epsilon_0 \frac{Aa}{dd_g}. \tag{W15.1}$$

Since $a \gg d_g$, this results in a substantial increase in C.

Capacitor design involves other issues beside having large capacitance. Dissipation is a major concern, and dc conductivity is another. Ion migration can cause currents to flow. These often involve defects, such as oxygen vacancies, moving through the dielectric. The tunneling of electrons from granule to granule in the GBBL capacitors

TABLE W15.1 Properties of Relaxor Dielectrics

Relaxor Material[a]			Transition $T_c(^\circ C)$	ϵ_r(max)
$Pb(Fe_{1/2}Nb_{1/2})O_3$	PFN	FE	112	24,000
$Pb(Mg_{1/3}Nb_{2/3})O_3$	PMN	FE	−0.8	18,000
$Pb(Mg_{1/2}W_{1/2})O_3$	PMW	AF	39	300
$Pb(Zn_{1/3}Nb_{2/3})O_3$	PZN	FE	140	22,000
$PbTiO_3$	PT	FE	490	8,000
$BaTiO_3$	BT	FE	130	12,000
	PLZT	FE	140	12,000

Source: Data from Y. Yamashita, *Am. Ceram. Soc. Bull.*, **73**, 74 (1994).

[a]FE and AF stand for ferroelectric and antiferroelectric transitions, respectively. The composition of PLZT is given by $Pb_{1-x}La_x(Zr_yTi_{1-y})_{1-x/4}O_3$, with $x = 0.07$ and $y = 0.65$.

provides a conduction mechanism. When working with granular materials a concern is the charging of the grains. For small enough granules, the discrete nature of the electronic charge plays an important role in determining the $I-V$ characteristics.

Another concern relates to the variation of capacitance with temperature. Often, circuits are used in which the stability of the RC time constant plays an important role. Since resistance of semiconductors drops with increasing temperature, it could be compensated for by finding a capacitor whose capacitance rises with increasing T. Relaxor materials often have such positive temperature coefficients.

W15.2 Substrates

Substrates are insulators that serve as the foundation upon which microcircuits are supported. Typical materials include alumina, aluminum nitride (both plain and diamond-coated), boron nitride, diamond thin films, mullite, and polyimide films, as well as others. Usually, the Si wafer which serves as the template for Si devices is bonded to a substrate that provides mechanical support and thermal dissipation. Table W15.2 provides a list of some common materials. Patterns of deposited metals, semiconductors, and insulators that comprise the circuit are supported by the Si template. The electrical insulating properties of the substrate are reflected in high values for the electrical resistivity.

Generally, the coefficient of thermal expansion, α, should match that of the semiconductor so that thermal stresses may be minimized. For example, alumina and GaAs have values that are well matched (see Table W15.2). GaAs can be bonded onto alumina with a gold–tin solder. In addition, materials of high thermal conductivity, κ, such as

TABLE W15.2 Properties of Substrate Materials[a]

Substrate	Dielectric Constant ϵ_r (at 1 MHz)	Rupture Modulus RM[b] (MPa)	Coefficient of Thermal Expansion α (10^{-6} K^{-1})	Thermal Conductivity κ (W/m·K)	Processing Temperature T_{proc} (°C)	Resistivity ρ (Ω·m)
Al_2O_3	9.9	550	6.7	17	1500	10^{13}
SiC	9.7	186	4.5	135	2000	—
Si_3N_4	7.0	850	3.4	30	1600	10^{10}
AlN	8.8	300	4.5	180	1900	10^{11}
BeO	6.8	250	7.6	250	2000	—
Mullite	3.8	185	5	6	1400	$>10^{12}$
Cordeirite	5	500	3	2	—	10^{9}
Titania	170	291	7.1	10.4	—	—
Borosilicate glass	4.0	70	3	2	800	—
Quartz + borosilicate	7.9	150	7.9	16	850	—
Si	11.7	—	2.5	151	—	—
GaAs	—	—	6.5	54	—	10^{6}

Source: Data from L. M. Sheppard, Ceram. Bull., **70**, 1467 (1991)).

[a]Note that large variations of reported values appear in the literature.
[b]Fracture strength under a bending load.

AlN, permit heat to be dissipated rapidly. The mechanical strength of the substrate should be high so that it can withstand the thermal stresses. Of paramount importance are the ability to deposit metallic layers on the material and to be able to withstand whatever machining operations are involved.

In photolithography there is the need to blacken the substrate, so that it will not reflect stray light and damage the latent image being cast upon a VLSI circuit. Oxides of Co, Cr, Fe, Nb, Ta, Ti, W, and Zr serve to blacken AlN without diminishing its high thermal conductivity.

For high-speed switching operations it is desirable to have small capacitances, so that the RC time constant will be small. This necessitates using substrates with small dielectric constants, preferably with $\epsilon_r < 5$. To this end, porous glasses may be used, with $\epsilon_r \approx 2$, although the presence of pores mechanically weakens the substrate. Boron phosphate glass ceramics offer materials with $\epsilon_r \approx 4$ and have very high resistivity, $\approx 10^{14}$ Ω·m. One may also use layered structures, making use of the fact that for capacitors in series, $C_{\text{total}} < \min(C_1, C_2, \ldots)$. For example, fluorohectorite is a synthetic mica silicate with layers separated from each other by sheets of hydrated cations. One may place layers of low-ϵ polymer between the sheets to form a low-capacity microstructure. Since the packaging of a VLSI chip also contributes to the capacitance, materials with low dielectric constants should be employed. Such materials as Teflon, polyimides, and benzocyclobutenes are often utilized.

W15.3 First-Order Ferroelectric Phase Transitions

First-order transitions may be handled by returning to Eq. (15.29) of the textbook[†] and assuming that $c > 0$ and $b < 0$. In place of Eq. (15.30), one has

$$\frac{\partial g}{\partial P} = a_0(T - T_0)P + bP^3 + cP^5 = 0. \tag{W15.2}$$

There now exists a temperature T_C such that for $T > T_C$, the minimum value of g is g_0 and there is no spontaneous polarization (i.e., $P = 0$). To determine T_C, the equations $\partial g/\partial P = 0$ and $g = g_0$ are solved simultaneously, giving

$$T_C = T_0 + \frac{3b^2}{16a_0c}, \tag{W15.3}$$

$$P = P(T_C) = \pm\sqrt{-\frac{3b}{4c}}. \tag{W15.4}$$

Note that the order parameter undergoes a discontinuity as the temperature is lowered below T_C. For temperatures below T_C, the spontaneous polarization is given by

$$P = \pm\sqrt{-\frac{b}{2c} + \sqrt{\frac{b^2}{4c^2} - \frac{a_0}{c}(T - T_0)}}. \tag{W15.5}$$

[†] The material on this home page is supplemental to *The Physic and Chemistry of Materials* by Joel I. Gersten and Frederick W. Smith. Cross-references to material herein are prefixed by a "W"; cross-references to material in the textbook appear without the "W."

The dielectric constant is obtained as before. For $T > T_C$

$$\epsilon_r = 1 + \frac{1}{\epsilon_0 a_0 (T - T_0)}, \tag{W15.6}$$

which is the same as in Eq. (15.35), but remains finite at $T = T_C$. For $T < T_C$ one finds that

$$\epsilon_r = 1 + \frac{1}{4\epsilon_0 c x (x - b/2c)}, \tag{W15.7a}$$

where

$$x = \sqrt{\frac{b^2}{4c^2} - \frac{a_0}{c}(T - T_0)}. \tag{W15.7b}$$

Since $b < 0$, this remains finite at $T = T_0$.

The extension to three dimensions may be obtained by writing the Gibbs free-energy density in a form consistent with cubic symmetry:

$$g = g_0 - \mathbf{E} \cdot \mathbf{P} + \frac{a}{2}P^2 + \frac{b}{4}P^4 + \frac{b' - b}{2}(P_y^2 P_z^2 + P_z^2 P_x^2 + P_x^2 P_y^2) + \frac{c}{6}P^6 + c'[P_x^4(P_y^2 + P_z^2) + P_y^4(P_z^2 + P_x^2) + P_z^4(P_x^2 + P_y^2)] + c'' P_x^2 P_y^2 P_z^2 + \cdots \tag{W15.8}$$

where $\mathbf{E}$ is the electric field vector. Matters may be simplified by letting $c' = 0$ and $c'' = 0$. As before, one begins with $\mathbf{E} = 0$. At the minimum value of g, three conditions apply:

$$\frac{\partial g}{\partial P_x} = P_x[a + bP^2 + (b' - b)(P_y^2 + P_z^2) + cP^4] = 0, \tag{W15.9a}$$

$$\frac{\partial g}{\partial P_y} = P_y[a + bP^2 + (b' - b)(P_z^2 + P_x^2) + cP^4] = 0, \tag{W15.9b}$$

$$\frac{\partial g}{\partial P_z} = P_z[a + bP^2 + (b' - b)(P_x^2 + P_y^2) + cP^4] = 0, \tag{W15.9c}$$

Various extrema may be identified. The first is at $(P_x, P_y, P_z) = (0, 0, 0)$, at which point the crystal has cubic symmetry and $g = g_0$. A second solution occurs at $(P_x, P_y, P_z) = (0, 0, \pm|P_z|)$, in which case

$$|P_z| = \sqrt{-\frac{b}{2c} + \rho\sqrt{\left(\frac{b}{2c}\right)^2 - \frac{a}{c}}}, \tag{W15.10}$$

where $\rho = \pm 1$. This solution corresponds to the breaking of cubic symmetry. There exists a spontaneous polarization, and the crystal has tetragonal symmetry. (Equivalent solutions follow from the cyclical permutation of P_x, P_y and P_z.) The reality of this solution requires that $b^2 > 4ac$. If $b < 0$, then $\rho = +1$ is always possible whereas if $b > 0$, then $\rho = -1$ is always possible. If $a < 0$ and $b < 0$, then $\rho = -1$ can also

occur. If $a < 0$ and $b > 0$, then $\rho = +1$ is another possibility. The Gibbs free-energy density at the extrema is given by

$$g = g_0 - \frac{ba}{12c} + \left(\frac{a}{3} - \frac{b^2}{12c}\right) P_z^2. \tag{W15.11}$$

If this Gibbs free-energy density lies below g_0, it will be the preferred thermodynamic state. Note that due to the symmetry of the solution, the parameter b' does not appear in Eq. (W15.10) or (W15.11).

For $E_z \neq 0$ the dielectric constant is determined approximately as before by solving

$$\frac{\partial g}{\partial P_z} = P_z(a + bP_z^2 + cP_z^4) - E = 0. \tag{W15.12}$$

For the cubic case the result expressed in Eq. (W15.6) is found.

For the tetragonal case

$$\epsilon_r = 1 + \frac{1}{4\epsilon_0 c}\left[\left(\frac{b}{2c}\right)^2 - \frac{a}{c} - \rho\sqrt{\left(\frac{b}{2c}\right)^2 - \frac{a}{c}}\right]^{-1/2}. \tag{W15.13}$$

Note that the dielectric constant diverges as b^2 approaches 4ac.

W15.4 Nonvolatile Ferroelectric Random-Access Memory

Computer random-access memory (RAM) currently employs semiconductor technology. One major drawback is that the information stored in RAM is lost in the event of a power failure or other sudden shutdown of the computer. A remedy for this is the use of nonvolatile ferroelectric random-access memory (NVFRAM). Ferroelectric domains are used to store the bits of information. A binary 1 corresponds to the electric polarization vector, **P**, pointing in one direction and a binary 0 to **P** pointing in the opposite direction. Since the polarization within a domain is determined by ionic displacements within the unit cells, domain walls typically propagate at speeds characteristic of ionic motion (i.e., the speed of sound, $c_s \sim 10^3$ m/s). For a domain of size $L \sim 1$ μm, this translates into a switching time of $L/c_s \sim 1$ ns. In addition to their nonvolatility, NVFRAMs can be written and erased many times (10^9–10^{13}) without degradation of switching polarization (fatigue), have low leakage currents, and retain their polarization state for a long time.

Many phenomena appearing in ferroelectrics have analogs in ferromagnetism. In particular, the hysteresis loops of ferroelectricity, obtained when P is plotted against the electric field, E, are analogous to the hysteresis loops of ferromagnetism, in which the magnetization, M, is plotted as a function of the magnetic intensity, H. The latter case is studied in some detail in Chapter 17, so only an abridged introduction to hysteresis is given here.

The hysteresis loop describes P as a double-valued function of E and is illustrated in Fig. W15.1. Suppose that initially all the electric dipole moments of a domain are aligned by applying a strong electric field. The value of the polarization vector will then be $P_{\text{sat}} = n\mu$, where n is the number of unit cells per unit volume and μ is the electric-dipole moment of a unit cell. Upon lowering E to zero, the polarization drops to a value P_{rem}, called the *remanent polarization*. Thus, even in the absence of an electric

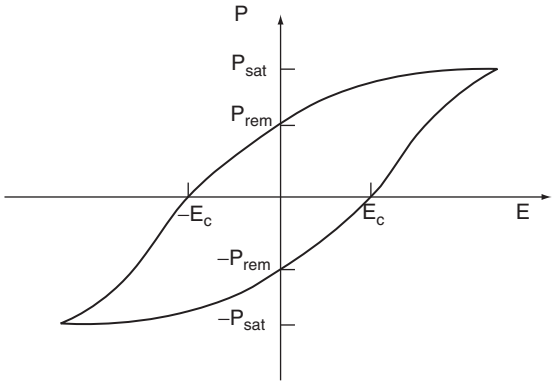

Figure W15.1. Ferroelectric hysteresis loop.

field, the polarization state is preserved and P_{rem} can serve as the binary 1 bit of the state of memory. This is what provides the nonvolatility of the memory. If the field is made more negative, the polarization will finally be zero at a value $E = -E_c$, where E_c is called the *coercive field*. If the field is made strongly negative, the polarization ultimately saturates at $-P_{\text{sat}}$. Reversing the process, and making $E = 0$, leads to a polarization $-P_{\text{rem}}$. This can represent the binary 0 of a state of memory. Increasing E to the value $+E_c$ removes the polarization, and making it strongly positive restores the saturation polarization P_{sat}. The net work done in going around the hysteresis loop is the area enclosed by the loop, $\oint E\,dP$, and is dissipated as heat.

In practical memory chips there are a large number of cells present on a surface array. Each domain is defined by the intersection of two conducting strips, one called the *word line* and the other called the *bit line*. To write a given bit, half the switching voltage is applied across the word line and half across the bit line, thus creating P_{rem}. To read a given bit, a switching voltage is applied. Half of it is supplied by the word line and half by the bit line, as in the writing case. If the cell is polarized in the $+P_{\text{rem}}$ state and a positive voltage is applied, a relatively small change in the polarization occurs, $P_{\text{sat}} - P_{\text{rem}}$. If the cell is in the $-P_{\text{rem}}$ state and a positive voltage is applied, a polarization change $P_{\text{sat}} + P_{\text{rem}}$ occurs. The resulting polarization current $J_P = -\partial P/\partial t$ produces a transient sensing voltage that may be detected and compared with that of a standard domain which is always switched from the + state. After reading the bit, the domain polarization is restored to its initial state by applying the appropriate electric field.

One problem is to prevent the polarization state of one domain from interacting with neighboring domains (i.e., *cross-talking*). Isolation transistors are inserted between domains to prevent this from happening.

Ferroelectrics currently used in NVFRAMs include the perovskite PZT [$Pb(Zr_xTi_{1-x})O_3$, with $x \approx 0.53$] and the layered perovskites SBT ($SrBi_2Ta_2O_9$) and SNT ($SrBi_2Nb_2O_9$). In the SBT crystal structure the unit cell consists of a stack along the c axis consisting of alternating $SrTa_2O_6$ perovskite blocks and planes of atoms containing Bi_2O_3. Typical parameters for some of these materials are $P_{\text{rem}} = 0.4$ C/m^2 and $E_c = 2800$ to 5000 kV/m for PZT, and $P_{\text{rem}} = 0.18$ C/m^2 and $E_c = 4500$ kV/m for SBT. The values depend on film thickness and the method of processing. The choice of proper electrode materials is of importance in decreasing the fatigue of the devices, as it can have a substantial effect on the microstructure of

the ferroelectric. For example, the sandwich combination Pt/PZT/Pt fatigues rapidly, whereas RuO_2/PZT/RuO_2, deposited on a MgO(100) substrate, has little fatigue. Other electrodes include IrO_2 and (La,Sr)CoO_3. The presence of oxygen vacancies can lead to charge trapping, which can pin domain walls and locally shift P_{rem} and E_c.

W15.5 Quartz Crystal Oscillator

As in the case of a bell, a crystal of finite size will "ring" with a characteristic set of normal-mode frequencies when excited mechanically. In the case of a piezoelectric crystal, electric fields are used to provide the stimulus. The frequencies are given approximately by $\omega \sim c_s/L$, where c_s is a speed of sound and L is a typical dimension. Although any piezoelectric crystal may be used, α-quartz is most commonly employed, and attention here is restricted to it. Oscillators with frequencies in the megahertz range are fabricated routinely. They are employed in clocks, computers, and radio transmitters and receivers. The quartz-crystal monitor is a basic tool for measuring thin-film deposition rates of adsorbates.

The nature of the modes of excitation of the crystal is determined by the shape of the cuts relative to the unit cell. The cuts are specified in terms of the dimensions of a rectangular parallelipiped of (thickness, length, width) $= (t, l, w)$, axes of rotation (x, y, z), and Euler angles of rotation of the parallelipiped relative to the crystal axes (ϕ, θ, ψ). The notation for the crystal cut is $xyz(t, l, w)\phi\theta\psi$. Various cuts are in use, labeled by the notation AT, BT, CT, DT, ET, GT, MT, NT, and so on. These cuts are special in that the piezoelectric coefficients are, to a first approximation, independent of temperature. Figure W15.2 shows a quartz crystal along with the directions of some of the cuts.

It should be noted that quartz is an example of an enantiomorphous crystal, which means that there are two independent but equivalent structures which are the mirror images of each other, referred to here as *right-* and *left-handed quartz*.

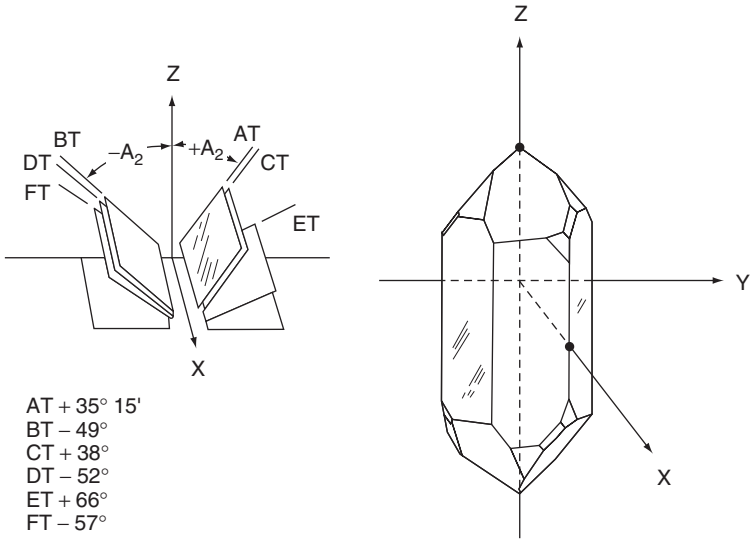

Figure W15.2. Quartz crystal along with some of the cuts used to create oscillator crystals. (Adapted from R. A. Heising, *Quartz Crystals for Electrical Circuits*, Van Nostrand, New York, 1946.)

The normal-mode frequencies are determined by solving the elastic equations of motion as in Section 10.10. To be more general, the expanded notation of Eq. (10.13) will be used, so

$$\rho\frac{\partial^2 u_\alpha}{\partial t^2} = -\rho\omega^2 u_\alpha = \sum_\beta \frac{\partial \sigma_{\alpha\beta}}{\partial x_\beta} = \sum_{\beta\mu\nu} C_{\alpha\beta\mu\nu}\frac{\partial \varepsilon_{\mu\nu}}{\partial x_\beta}, \tag{W15.14}$$

where ρ is the density, $\mathbf{u}$ the displacement, $\sigma_{\alpha\beta}$ the stress tensor, $\varepsilon_{\mu\nu}$ the strain tensor, and $C_{\alpha\beta\mu\nu}$ the elastic coefficient tensor. All indices run from 1 through 3. The boundary conditions are that the normal components of the stress tensor vanish on the surface:

$$\sum_\beta \sigma_{\alpha\beta}\hat{n}_\beta = 0. \tag{W15.15}$$

Quartz (a trigonal or rhombohedral crystal) has the (symmetric) elastic coefficient tensor (in reduced notation)

$$\mathbf{C} = \begin{bmatrix} C_{11} & C_{12} & C_{13} & C_{14} & 0 & 0 \\ \cdot & C_{11} & C_{13} & -C_{14} & 0 & 0 \\ \cdot & \cdot & C_{33} & 0 & 0 & 0 \\ \cdot & \cdot & \cdot & C_{44} & 0 & 0 \\ \cdot & \cdot & \cdot & \cdot & C_{44} & C_{14} \\ \cdot & \cdot & \cdot & \cdot & \cdot & 2(C_{11}-C_{12}) \end{bmatrix} \tag{W15.16}$$

where $(C_{11}, C_{12}, C_{13}, C_{14}, C_{33}, C_{44}) = (8.68, 0.71, 1.19, 1.80, 10.59, 5.82) \times 10^{10}$ Pa. The density is $\rho = 2649$ kg/m^3. The piezoelectric tensor is

$$\mathbf{d} = \begin{bmatrix} d_{11} & -d_{11} & 0 & d_{14} & 0 & 0 \\ 0 & 0 & 0 & 0 & -d_{14} & -2d_{11} \\ 0 & 0 & 0 & 0 & 0 & 0 \end{bmatrix}, \tag{W15.17}$$

with $(d_{11}, d_{14}) = (2.3, -0.67)$ pm/V (for right-handed quartz). For left-handed quartz the signs of d_{11} and d_{14} are opposite. The dielectric constant tensor is

$$\varepsilon_r = \begin{bmatrix} \varepsilon_1 & 0 & 0 \\ 0 & \varepsilon_1 & 0 \\ 0 & 0 & \varepsilon_2 \end{bmatrix} \tag{W15.18}$$

with $(\varepsilon_1, \varepsilon_2) = (4.34, 4.27)$. The coefficients of linear expansion are described by the tensor

$$\boldsymbol{\alpha} = \begin{bmatrix} \alpha_1 & 0 & 0 \\ 0 & \alpha_1 & 0 \\ 0 & 0 & \alpha_2 \end{bmatrix} \tag{W15.19}$$

with $(\alpha_1, \alpha_2) = (14.3, 7.8) \times 10^{-6}$ K^{-1}.

After solving the wave equation, expressions for the various modes are obtained. Consider here one such mode. The AT-cut $(\phi, \theta, \psi) = (-90^\circ, 35^\circ 15', 90^\circ)$ crystal has

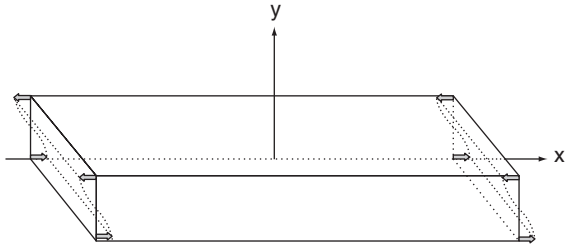

Figure W15.3. Shear oscillation of a quartz crystal oscillator. (Adapted from R. A. Heising, *Quartz Crystals for Electrical Circuits*, Van Nostrand, New York, 1946.)

a mode that undergoes a shear oscillation described by the equation

$$u_x(y,t) = U_0 \cos\frac{n\pi y}{d} e^{-i\omega_n t}, \tag{W15.20}$$

where U_0 is the amplitude and

$$\omega_n = n\frac{\pi}{d}\sqrt{\frac{C_{66}}{\rho}}, \qquad n\ odd. \tag{W15.21}$$

The thickness of the slab is denoted by d. This formula implies a wave speed of $c_s = \sqrt{C_{66}/\rho} = 7757$ m/s for quartz, using $C_{66} = 2(C_{11} - C_{12})$. The vibrational motion is depicted in Fig. W15.3.

One of the main problems with the crystal oscillator is that the resonant frequency changes with temperature, due to thermal expansion and a temperature variation of the elastic constants. One may describe the frequency drift over a restricted range by the linear formula $\Delta f/f_0 = a(T - T_0)$, where a is called the *temperature coefficient*. The size of the parameter a depends on the nature of the crystal cut. For example, in AT-cut quartz, if $T_0 = 43°\text{C}$, then $a = 0$ in the neighborhood of $T = T_0$. This makes the AT oscillator stable against (small) temperature fluctuations. The various popular crystal cuts have different temperatures at which they attain optimum thermal stability. Thermistors operating in conjunction with microprocessors can now accurately compensate for the thermal drift of these oscillators and the precise cutting of crystals is less necessary than it once was.

One interesting application of crystal oscillators is for use as a thickness monitor for vapor-deposition technology. A layer of adsorbed material on the surface of a crystal oscillator increases the system's inertia and lowers the resonant frequency by an amount proportional to the additional mass. Thus, for the quartz-crystal deposition monitor (QCM), an adlayer of Al on an AT-cut slab with a resonant frequency of 6 MHz will shift the resonant frequency by 22.7 Hz per nanometer of adsorbate. With precision-counting electronics, such shifts are readily measurable.

W15.6 Lithium-Ion Battery

The need for a compact reliable battery for computers, watches, calculators, and implantable medical devices has prompted the invention of the lithium-ion battery. Early batteries did not carry enough energy per unit mass. For

example, the lead-acid battery can provide only ≈ 35 W·h/kg (70 W·h/L) and the Ni/Cd battery ≈ 25 W·h/kg (100 W·h/L). In contrast, the Li battery provides ≈ 200 W·h/kg (250 W·h/L), as compared with gasoline, which can provide $\approx$ 15,000 W·h/kg of thermal energy (1 W·h = 3600 J). Any battery has mass and occupies a volume. For some applications mass is the more crucial parameter, so one rates the battery in terms of W·h/kg. In other applications volume may be more crucial, so the rating in terms of W·h/L is more relevant.

The Li battery consists of three parts: the anode (lithium), the electrolyte, and the cathode. Since Li reacts strongly with aqueous solutions, the electrolyte is a liquid that must be aprotic (not contain hydrogen ions). Ideally, one would want an electrolyte with a high solubility for lithium salts and a high mobility for the ions. This involves the use of electrolytes with high dielectric constants and low viscosities. Both of these effects are understandable in terms of elementary physics.

When an ion of charge q is placed in a solvent, there is an electrostatic lowering of its energy by the Born solvation energy. This is illustrated in Fig. W15.4, which shows the solvent molecules as dipoles which become locally aligned with the electric field of the ion. Assuming that a solvation hole of radius a is produced around the ion, the solvation energy is $U = (1 - 1/\epsilon_r)q^2/8\pi\epsilon_0 a$. With large ϵ_r the solvation energy is increased. In addition, a large value of ϵ_r implies that ions are shielded from each other's influence by the polarization charge that gathers around the ions. The ions are less likely to impede each other's motion at high concentrations.

An applied electric field $\mathbf{E}$ leads to a steady-state ionic velocity $\mathbf{v}_i = \mu_i \mathbf{E}_i$, where μ_i is the ith ion's mobility. The net conductivity is $\sigma = \Sigma n_i q_i \mu_i$, where n_i, q_i, and μ_i are the concentration, charge, and mobility of the respective ions. Neglecting ion–ion interactions, the electric force and the Stokes viscous force on a given ion cancel at equilibrium. Thus $q_i\mathbf{E} - 6\pi\eta r_i \mathbf{v}_i = 0$, where η is the viscosity of the liquid and r_i is the ionic radius (including whatever "hydration" shell accompanies it). Thus

$$\mu_i = \frac{q_i}{6\pi\eta r_i}. \tag{W15.22}$$

The lower the viscosity of the electrolyte, the higher the mobility of the ions and the lower the internal resistance of the battery. Consider an electrolyte of thickness L and cross-sectional area A. The internal resistance is computed by regarding each ionic

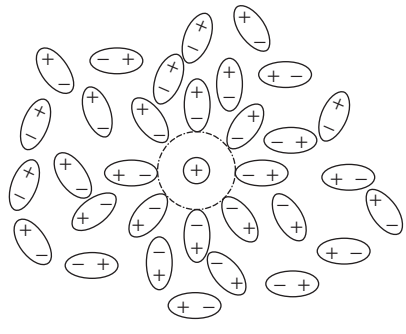

Figure W15.4. Dipoles of the solvent become polarized by the ion.

TABLE W15.3 Electrolyte Solvents[a]

Electrolyte Solvent	Dielectric Constant ϵ_r	Viscosity η (cp)	Temperature (°C) Melting T_m	Boiling T_b
Acetonitrile (AN)	38	0.35	−46	82
Dimethoxyethane (DME)	7.2	0.46	−58	84
N,*N*-Dimethylformate (DMF)	37	0.80	−61	158
Methylformate (MF)	65	0.63	−99	32
Propylene carbonate (PC)	64	2.53	−49	241
Nitromethane (NM)	36	0.62	−29	101
Dimethylsulfite (DMSI)	23	0.77	−141	126
Tetrahydrofuran	7.6	0.46	−109	66
Ethyl acetate (EC)	6.0	0.44	−84	77

Source: Data from H. V. Venkatasetty, ed., *Lithium Battery Technology*, Wiley, New York, 1984.

channel as operating in parallel with the others, so

$$\frac{1}{R_{\text{int}}} = \sum_i \frac{1}{R_i} = \sum_i \frac{A}{L}\sigma_i = \frac{A}{6\pi\eta L}\sum_i \frac{n_i q_i^2}{r_i} \tag{W15.23}$$

Clearly, a low viscosity favors a low internal resistance.

In Table W15.3 data are presented relevant to some of the common organic solvents used in conjunction with lithium salts as electrolytes for lithium batteries. The melting and boiling temperatures (T_m and T_b) define the temperature limits for the electrolyte remaining a liquid.

The electrolyte consists of salt dissolved in the organic solvent. Typical salts employed are LiCl, LiBr, LiI, $LiAsF_6$, LiSCN, $LiNO_3$ and $LiClO_4$. See also Fig. 14.14, which describes the use of $p(EO)_9LiCF_3SO_3$ as a polymer electrolyte. Both the Li^+ and the corresponding negative ions contribute to the electrical current. Interestingly enough, the negative ion often has the higher mobility, despite the fact that its bare radius is larger than that of the positive ion. The reason has to do with the "hydration" shell. Positive ions, being smaller, bind solvent ions more effectively than do negative ions. The solvated ion moves as a unit. Typically, the negative ion may have twice the mobility of the positive ion.

Some common cathode materials employed are CF_x, CuO, CuS, FeS, FeS_2, MnO_2, MoS_2, V_6O_{13}, $SOCl_2$, V_2O_5, and $Bi_2Pb_2O_5$. Often, these are intercalated into graphite or another binder. In Table W15.4 typical battery systems are listed along with their open-circuit voltage and operating voltages. Also listed are the energy densities stored in the batteries. The open-circuit voltages, V_{open}, are determined by the difference in the standard electrode potentials between the cathode and the anode (see Section W12.4, where corrosion is discussed).

W15.7 Fuel Cells

Fuel cells (FCs) are batteries in which there is a continuous input of fuel and oxidizer and a corresponding output of electrical power as well as waste products and waste

TABLE W15.4 Common Lithium-Ion Battery Configurations

Cathode	Electrolyte	Open-Circuit Voltage V_{open} (V)	Operating Voltage V_{oper} (V)	Energy Density u (W·h/kg)
CF_x	DME/PC + $LiBF_4$	3.4	2.6	235
CuO	1,3-dioxolane	2.4	1.3	165
CuS	—	2.1	1.8	198
FeS	Li halide salts	1.4	1.3	105
FeS_2	$LiCF_3SO_3$ in solvent	1.9	1.5	220
MnO_2	—	3.3	2.8	150
MoS_2	PC/Ec + $LiAsF_6$	2.4	1.9	61
V_6O_{13}	PE + $LiClO_4$	3.3	3.0	200
$SOCl_2$	Thionyl chloride + $LiAlCl_4$	3.7	3.2	385
V_2O_5	ME + $LiAsF_6$ + $LiBF_4$	3.4	2.8	264

Source: Data from C. D. S. Tuck, ed., *Modern Battery Technology*, Ellis Horwood, New York, 1991.

heat. FCs were invented in 1836 by Sir William Grove. The present FCs operate on the inverse reaction to the electrolysis of water, $2H_2 + O_2 \rightarrow 2H_2O$, which is an exothermic reaction in the liquid phase with $\Delta G = -4.92$ eV. The cells offer the possibility of providing a clean and efficient energy source. The hope is that they will some day become inexpensive enough to be more widely used.

There are five basic designs for the cells: the alkaline fuel cell (AFC), the proton-exchange membrane fuel cell (PEMFC), the phosphoric acid fuel cell (PAFC), the molten-carbonate fuel cell (MCFC), and the solid-oxide fuel cell (SOFC). The operating temperature ranges for these cells are quite different. For the AFC, PEMFC, PAFC, MCFC, and SOFC devices, the temperature ranges are 60 to 200, 60 to 110, 150 to 210, 550 to 700, and 1000 to 1100°C, respectively. In the case of the MCFC and SOFC, elevated temperatures are needed to have sufficient ion mobility through the electrolyte.

A typical fuel cell is shown schematically in Fig. W15.5. In the PEMFC, hydrogen is convected through the anode and impinges on a platinum catalyst layer. The reaction $H_2 \rightarrow 2H^+ + 2e^-$ is exothermic when it occurs on the catalyst. The electrons flow into the external circuit and the protons diffuse into the proton-exchange membrane which

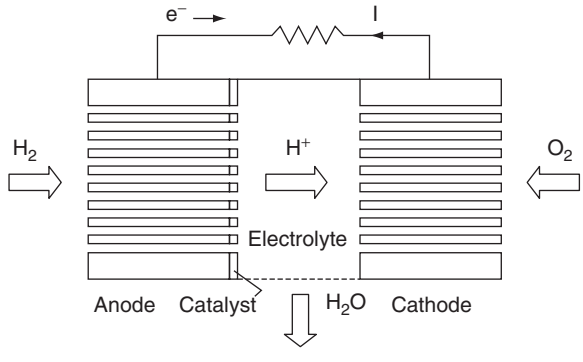

Figure W15.5. Prototype of a typical PEMFC fuel cell using hydrogen as the fuel.

serves as the electrolyte. The membrane is typically a material with a high proton conductivity, such as a sulfonated fluorocarbon polymer (NAFION), or the sulfonated styrene/ethylene–butylene/styrene copolymer. On the other side of the membrane is the cathode.† Oxygen diffuses in from the other side of the FC through the cathode and combines with the protons and the electrons returning from the circuit according to the reaction $4H^+ + O_2 + 4e^- \rightarrow 2H_2O$. Since there are four electrons pumped into the circuit for the reaction $2H_2 + O_2 \rightarrow 2H_2O$, the theoretical EMF for the hydrogen FC is $\epsilon = -\Delta G/4e = 1.23$ V. A fuel-cell generator generally consists of a stack of several hundred FCs with the batteries connected in series with each other.

The internal resistance of the FC limits the actual terminal voltage when a current is drawn from it. This is determined largely by the mean free path of the ions in the electrolyte as well as by whatever hydrodynamic constraints are placed on the flows. For example, a transition from laminar to turbulent flow for the hydrogen and oxygen flowing through the electrodes will impose a constraint on how rapidly fuel and oxidant may be delivered to the FC. In addition, thermally activated reverse reactions at the electrodes (such as $2H^+ + 2e^- \rightarrow H_2$ at the anode and $2H_2O \rightarrow 4H^+ + O_2 + 4e^-$ at the cathode) compete with the forward reactions, giving rise to what are called *exchange overpotentials*. These reactions act as batteries with reverse polarity in series with the FC.

The theoretical efficiency for the conversion of chemical energy to electrical energy in the FC is high. It may be computed from a knowledge of the enthalpy change $\Delta H = -5.94$ eV in the liquid phase and the Gibbs free energy change $\Delta G = -4.92$ eV. Since the waste heat is $Q = T\Delta S = \Delta H - \Delta G$, the efficiency is $\eta = \Delta G/\Delta H = 82.8\%$. Practical MCFCs have $\eta \approx 60\%$ and PAFCs have $\eta \approx 40\%$.

One of the requirements of the electrolyte is that it be impervious to the reactants but allow the ions to pass through with high conductivity. In the SOFC the electrolyte is ZrO_2/Y_2O_3 and it is the O^{2-} ion that diffuses through the electrolyte. In the MCFC the electrolyte is Li_2CO_3/K_2CO_3. The AFC uses KOH as the electrolyte and the PAFC uses phosphoric acid, H_3PO_4. In the AFC OH^- ions are the diffusing species, and in the MCFC they are the CO_3^{2-} ions.

One of the main problems with fuel cells is the preparation of the hydrogen fuel. Ideally, one would like to produce it from fuels such as methane by a process called *reforming*. The hydrogen could be stored temporarily in metal hydrides. Additional problems to FC design arise from poisoning of the catalysts by CO or CO_2.

REFERENCES

Batteries

Tuck, C. D. S., ed., *Modern Battery Technology*, Ellis Horwood, New York, 1991.

Venkatasetty, H. V., ed. *Lithium Battery Technology*, Wiley, New York, 1984.

Quartz-Crystal Oscillator

Heising, R. A., *Quartz Crystals for Electrical Circuits*, Van Nostrand, New York, 1946.

† Note that the term *anode* is used here as the electrode which acts as the source of positive charge inside the battery and negative charge outside the battery. This is opposite to the more conventional definition.

Nonvolatile Ferroelectric RAM

Auciello, O., J. F. Scott, and R. Ramesh, The physics of ferroelectric memories, *Phys. Today*, July 1998, 22.

Fuel Cells

Hoogers, G., Fuel cells: power for the future, *Phys. World*, Aug. 1998, 31.

Kartha, S., and P. Grimes, Fuel cells: energy conversion for the next century, *Phys. Today*, Nov. 1994, 54.

PROBLEM

W15.1 Consider the AT-cut quartz-crystal deposition monitor. Let c_s denote the speed of sound in quartz. Derive the formula for the shift of resonant frequency of the oscillator, Δf, when an adlayer of thickness δ and mass density ρ_a is deposited on the surface:

$$\frac{\Delta f}{f} = f\frac{\delta}{c_s}\frac{\rho_a}{\rho},$$

where ρ is the density of quartz.